# *Supporting Information*

## High Efficiency Near-Infrared Light Emission and Ultra-high Stability Lead-free Double Perovskite $Cs_2Na_{1-x}Ag_xBi_{1-y}Al_yCl_6$

Bin He,[a] Qilin Wei,[a] Bao Ke,[a] Zixuan Wu,[a] Hualin Zhao,[a] Jieyu Wei,[a] Chengzhi Yang,[a] Shuya Jin,[a] Bingsuo Zou[iD*a]

a School of Resources, environments and materials and School of Physical Science and Technology, Guangxi Key Lab of Processing for Nonferrous Metals and Featured Materials and Key lab of new Processing Technology for Nonferrous Metals and Materials, Ministry of Education, Guangxi University, Nanning 530004, China
Corresponding Authors:
zoubs@gxu.edu.cn (B.Z.)

## Experimental section

### Materials and Chemicals

Chemicals.Caesium chloride (CsCl, 99.99%, Aladdin), silver acetate (Ag(ac), 99.99%, Bidepharm), bismuth Trichloride ($BiCl_3$, 99.99%, Macklin), sodium chloride (NaCl, 99.99%, Macklin), manganese chloride ($AlCl_3 \cdot 6H_2O$, 99%, Aladdin). Hydrochloric acid (HCl, 36−38wt.% in water, Beijing Chemical Works), and absolute ethanol (AR, Beijing Tongguang Fine Chemical Co., Ltd., China) were purchased and used as received without further purification.

### Synthesis

In order to avoid the influence of impurities, first soak the polytetrafluoroethylene liner with aqua regia for 24 hours. Then, 2mmol CsCl, (1-x)mmol Na, x mmol Ag, (1-y) mmol Bi and y mmol Al were placed in a 25mL polytetrafluoroethylene autoclave, followed by 4ml hydrochloric acid solution. Then put the inner lining into a stainless-steel Parr autoclave, and heat the reaction in an oven at 180 °C for 10 hours. After the heating reaction is over, it is naturally cooled to room temperature.Then the prepared perovskite powder was filtered out, washed with absolute ethanol three times, and dried in a vacuum drying oven at 60 °C for 8 hours.Finally, samples of $Cs_2Na_{1-x}Ag_xBi_{1-y}Al_yCl_6$ perovskite polycrystalline at different doses were obtained.

## Measurement and Characterization

**Powder X-ray Diffraction (XRD):** The powder X-ray diffraction pattern was measured using a Cu Kα (λ = 0.71073 Å) radiation rotating anode and an X-ray diffractometer (model: SMARTLAB 3 KW) manufactured by Rigaku Corporation in

the 2θ range of 10°-75°.

**Absorbance:** Absorption spectra of the solid powder were measured with an UV-vis spectrophotometer (PerkinElmer Instruments, Lambda 750) at a range of 250 to 800 nm.

**Photoluminescence Measurements:** Use the HORIBA multifunctional fluorescence spectrometer test system to collect room temperature photoluminescence (PL), photoluminescence excitation (PLE) on the samples.

**Lifetime Measurements:** For emission lifetime measurement, the pulsed excitation light (350 nm) was generated by a μF2 60W xenon flash lamp. The detector signal was set below a threshold of 3000 counts per second. The lifetime of emission was determined by reconvolution fit with the instrument response function using the Edinburgh F1000 software. In all cases, emission decay was satisfactorily fitted with a multiple-exponential function until reconvolution with goodness-of-fit ($\chi$R2) in the range between 0.9and 1.2.

**Photoluminescence quantum yield Measurements:** The photoluminescence quantum yield (PLQY) was measured by HORIBA multifunctional fluorescence spectrometer test system, and the data were collected by placing the powder on a glass slide inside the integrating sphere.

**Raman Measurements:** A fast and confocal Raman imaging system (WITec alpha 300 R) was used to characterize the Raman spectrum of the sample with an excitation wavelength of 532 nm.

**SEM-EDS Measurements:** The morphology of the sample was characterized by a

Sigma 500 field emission scanning electron microscope, and the proportion of elements was characterized by energy dispersive X-ray spectroscopy from Oxford instruments.

**TGA (Thermogravimetric Analysis) Measurements:** The thermal stability of the sample was measured on a differential thermogravimetric (TGA) analyzer (DTG-60H) from RT to 800℃ under nitrogen atmosphere.

## Computational Methods:

All calculations at density functional theory are carried out using the Vienna Ab initio simulation package (VASP).[1-2] The generalized gradient approximation of the Perdew–Burke–Ernzerhof (PBE)[3] parameterization with projector-augmented wave[4] method are performed for the exchange and correlation functional. For all elements, ultra-soft pseudopotentials are used. The kinetic-energy cutoff of 300 eV and a 2×2×2 Monkhorst–Pack k-mesh for the wavefunction basis set is employed. The energy convergence criterion is set as $1.0\times10^{-5}$ eV for structural relaxations. The supercell structure containing 30 atoms of $Cs_2NaBiCl_6$ is constructed.

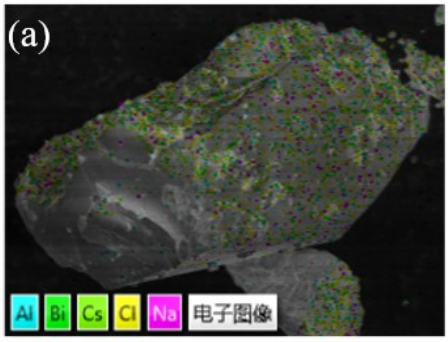
(a)
Al
Bi
Cs
Cl
Na
电子图像

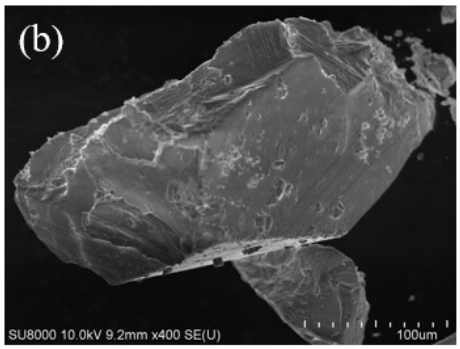
(b)
SU8000 10.0kV 9.2mm x400 SE(U)
100um

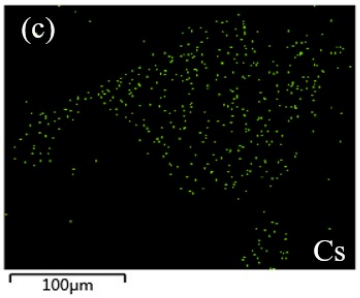
(c)
Cs
100μm

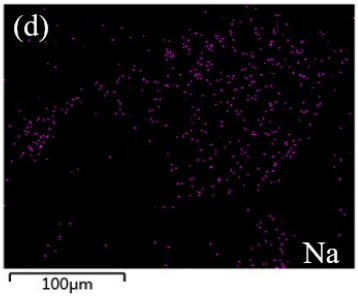
(d)
Na
100μm

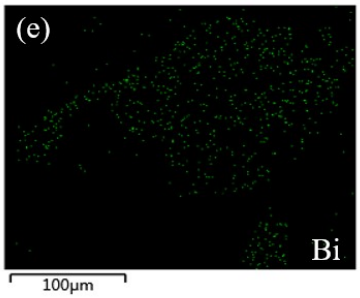
(e)
Bi
100μm

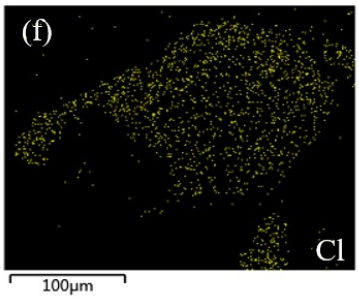
(f)
Cl
100μm

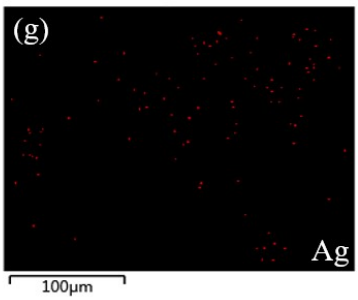
(g)
Ag
100μm

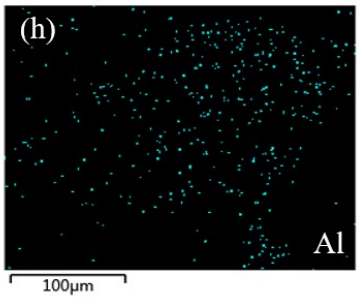
(h)
Al
100μm

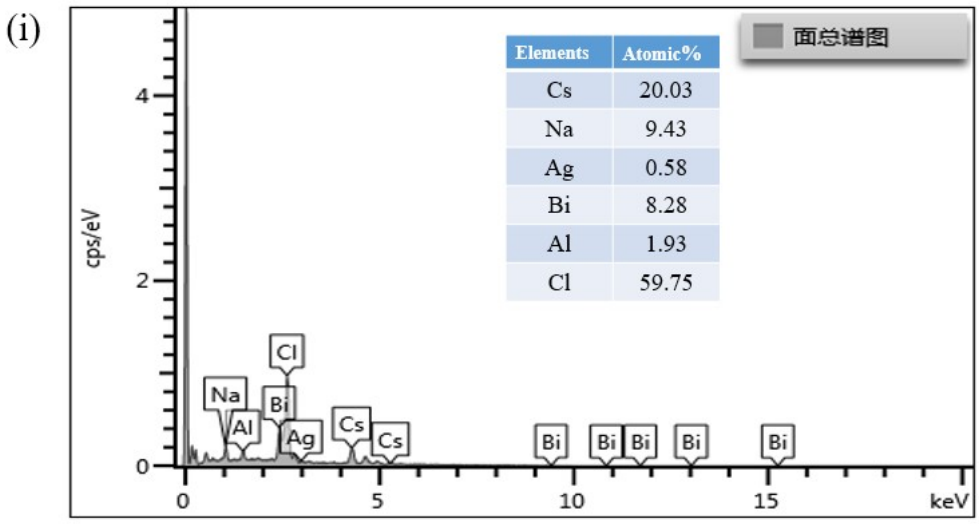


Fig S1 (a-b) EDS element stratified electronic image of $Cs_2Na_{1-x}AgxBi_{1-y}Al_yCl_6$ (x=0.05,y=0.2)and SEM image. (c-h) EDS element diagram of Cs, Na, Bi, Cl, Ag and Al in $Cs_2Na_{1-x}Ag_xBi_{1-y}Al_yCl_6$(x=0.05,y=0.2).(i) The corresponding EDS spectrum.

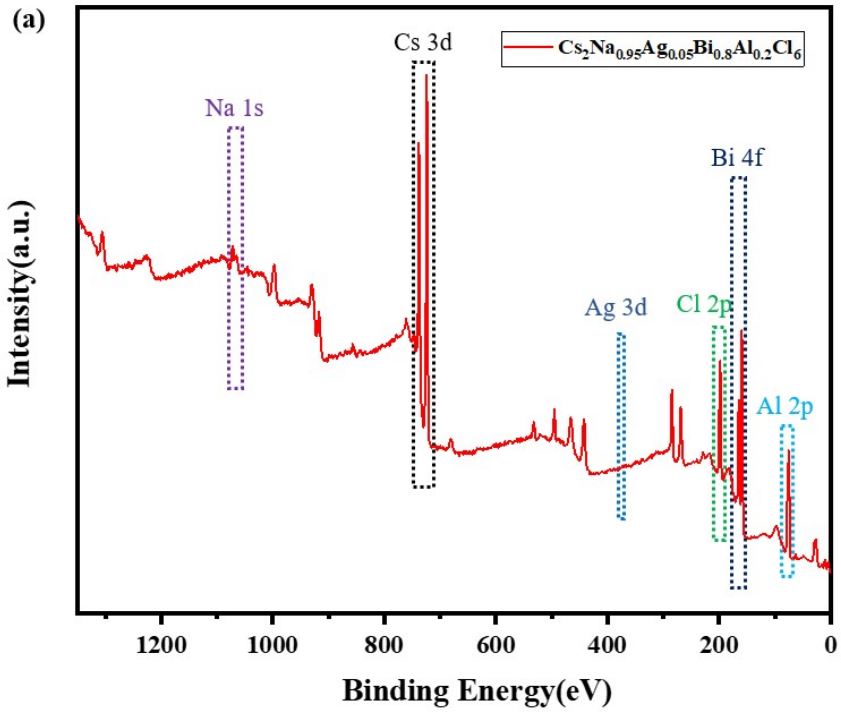

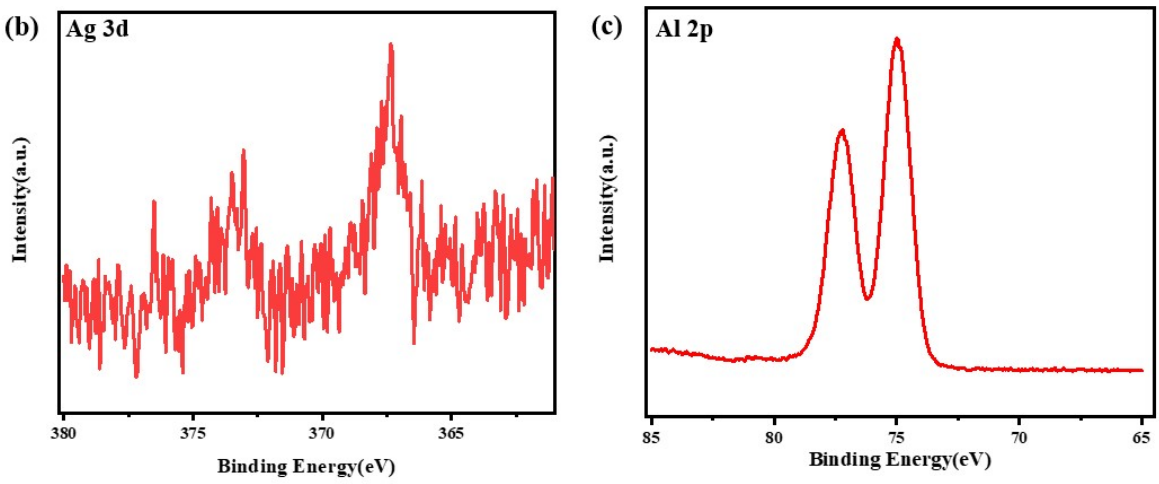


Fig S2 (a) $Cs_2Na_{0.95}Ag_{0.05}Bi_{0.8}Al_{0.2}Cl_6$ XPS spectra. (b) The characteristic peak of Ag, due to the low incorporation amount of silver, the curve of the peak is not smooth. (c) Characteristic peak of Al, indicating its complete incorporation.

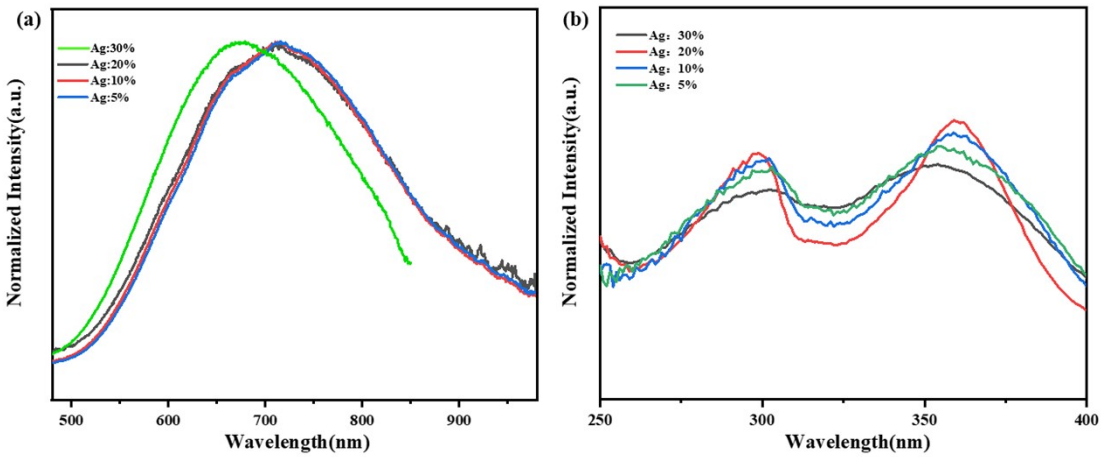


Fig S3 (a) PL spectra of $Cs_2Na_{1-x}Ag_xBi_{1-y}Al_yCl_6$ (x= 0.3,0.2,0.1,0.05;y=0.2)at different Ag concentrations.(b) PLE spectra of $Cs_2Na_{1-x}Ag_xBi_{1-y}Al_yCl_6$ (x= 0.3,0.2,0.1,0.05;y=0.2)at different Ag concentrations.

m

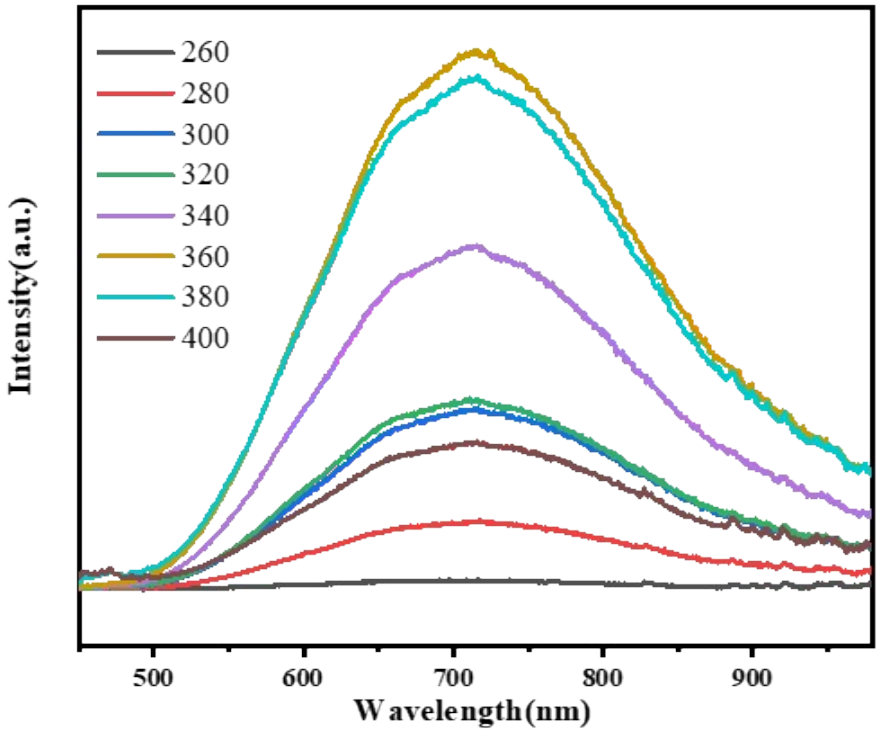


Fig. S4 PL spectra of Cs2Na1-xAgxBi1-yAlyCl6 in excited at 260 to 400nm.

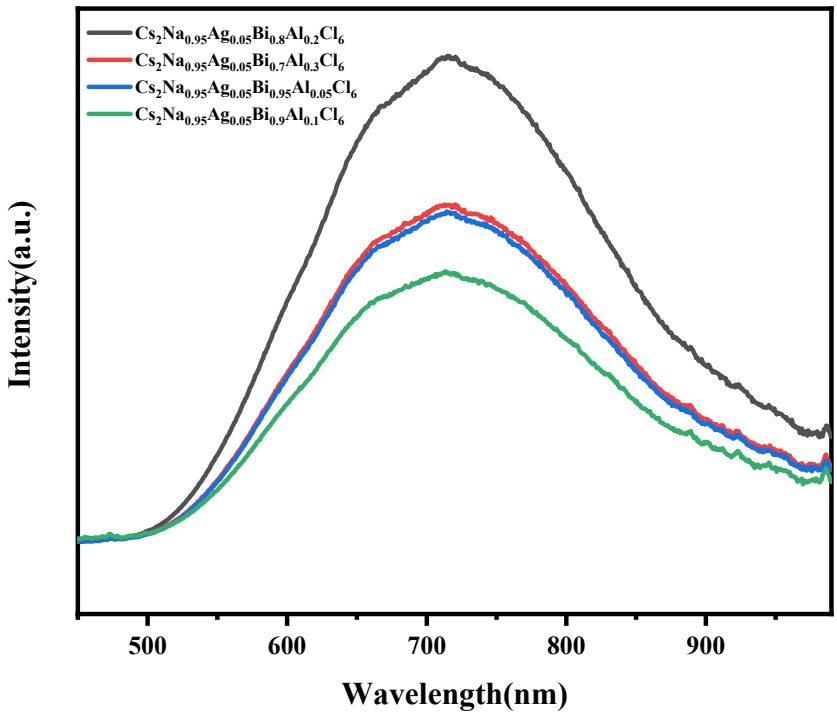


Fig S5 Present the emission spectra of the samples with varied Al ion concentration.

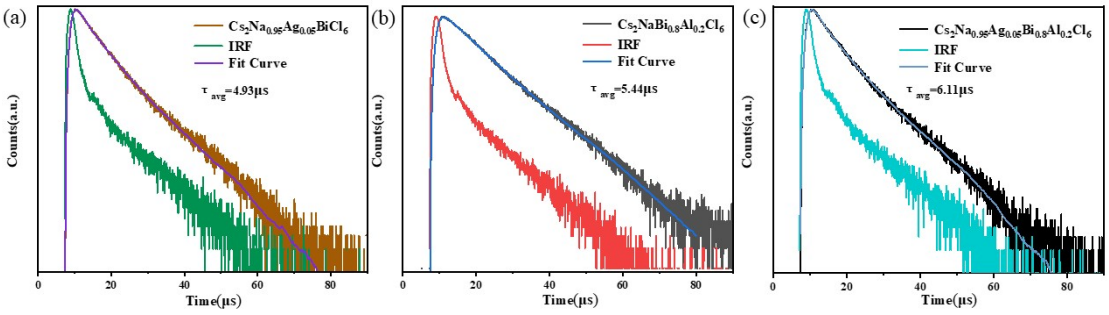


Fig S6 the PL lifetime decay curves of (a) $Cs_2Na_{0.95}Ag_{0.05}BiCl_6$, (b) $Cs_2NaBi_{0.8}Al_{0.2}Cl_6$ and (c) $Cs_2Na_{1-x}Ag_xBi_{1-y}Al_yCl_6$.

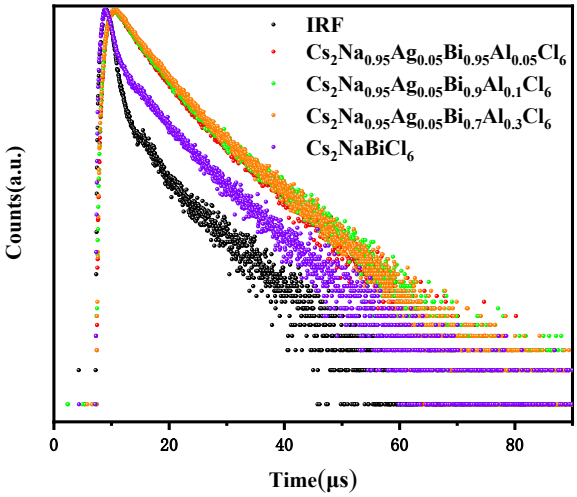


Fig S7 the PL lifetime decay curves of $Cs_2Na_{1-x}Ag_xBi_{1-y}AlyCl_6$(x=0.05) at different doped Al concentrations.

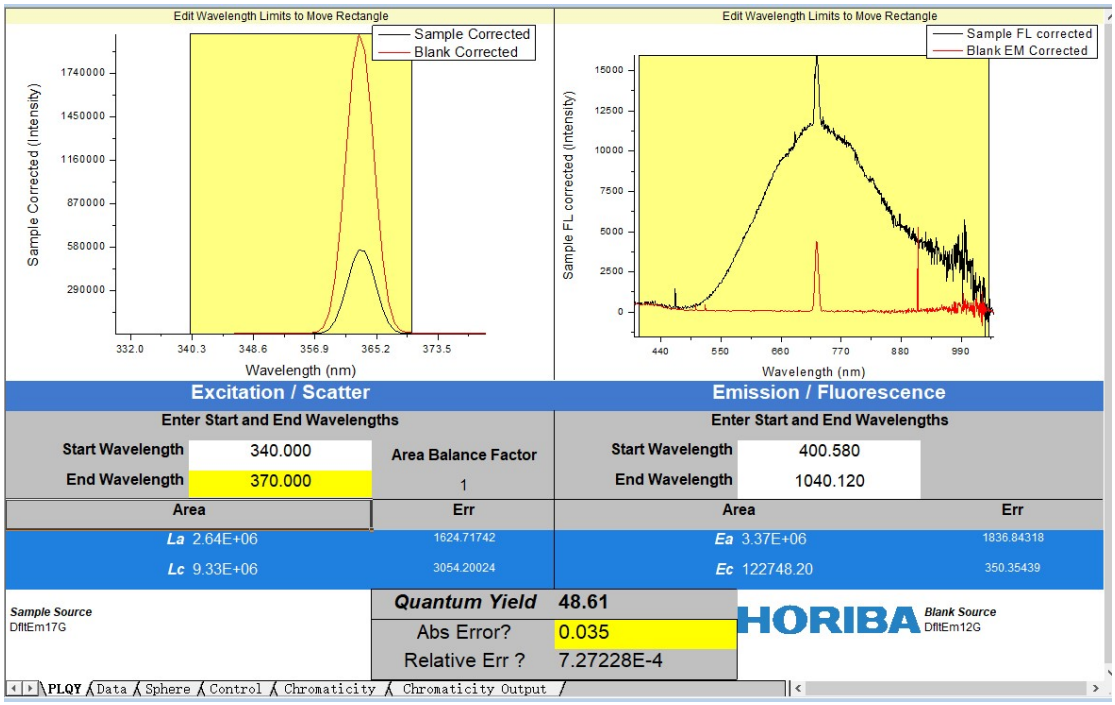


Fig S8 PLQY measurement of Cs2Na1-xAgxBi1-yAlyCl6(x=0.05,y=0.2).

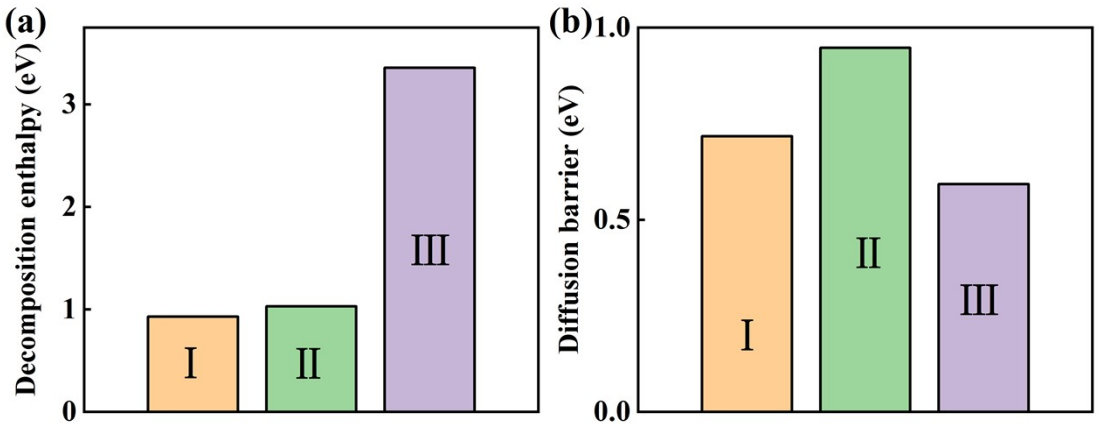


Figure S9. (a) Decomposition enthalpy of (Ⅰ)$Cs_2NaBiCl_6$, (Ⅱ) $Cs_2AgBiCl_6$ and (Ⅲ)$Cs_8Na_3AgAlBi_3Cl_{24}$ corresponding to the following reaction pathways: (I) $Cs_2NaBiCl_6 \rightarrow$ 2CsCl + NaCl + $BiCl_3$; (II) $Cs_2AgBiCl_6 \rightarrow$2CsCl + AgCl + $BiCl_3$; (III) $Cs_8Na_3AgAlBi_3Cl_{24} \rightarrow$ 8CsCl + 3NaCl + AgCl + $AlCl_3$+ 3$BiCl_3$ (b) Diffusion barrier of $V_{Cl}$ in (Ⅰ)$Cs_2NaBiCl_6$, (Ⅱ) $Cs_2AgBiCl_6$ and (Ⅲ)$Cs_8Na_3AgAlBi_3Cl_{24}$.

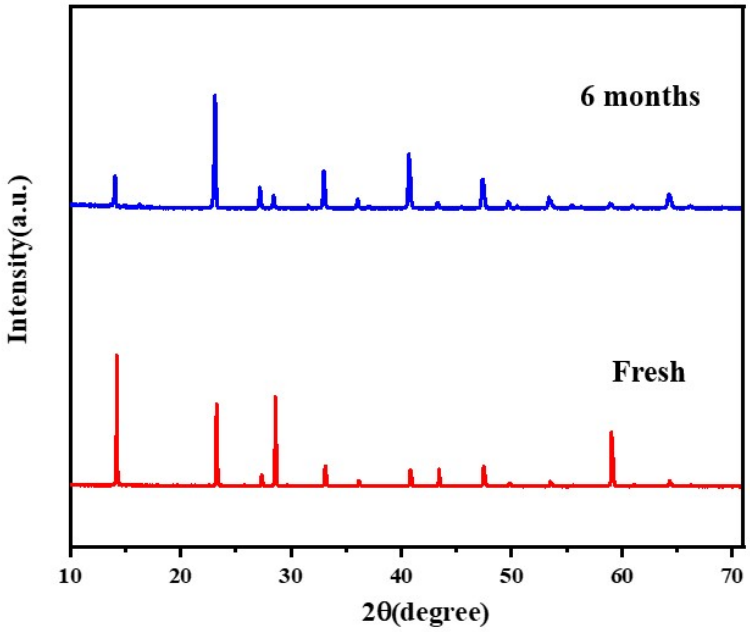


Fig S10 PXRD of Cs2Na1-xAgxBi1-yAlyCl6(x=0.05,y=0.2) samples after six months of storage.

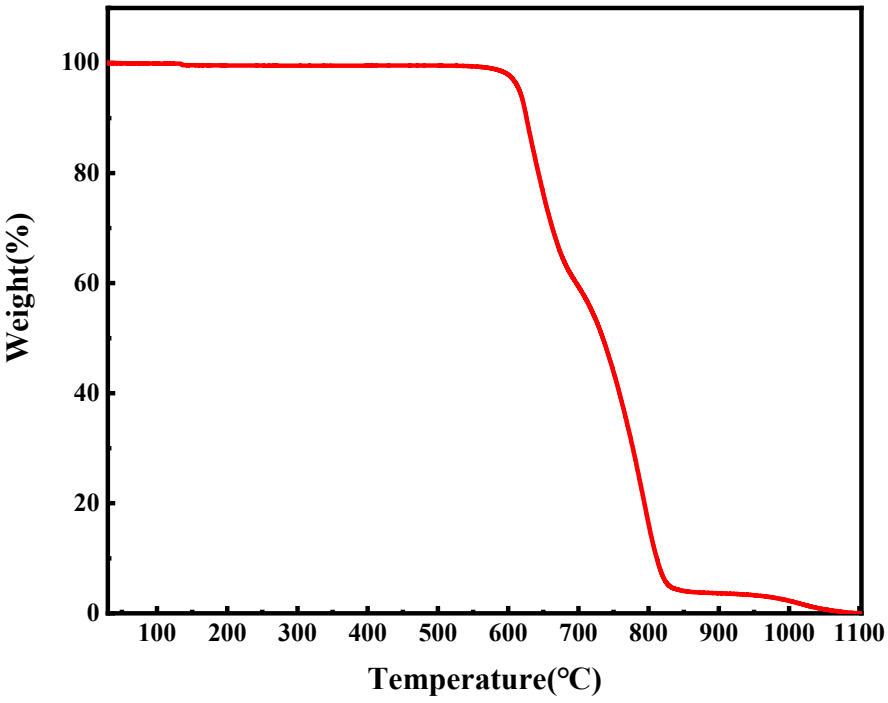


Fig S11 Thermogravimetric analysis (TGA) of $Cs_2Na_{1-x}Ag_xBi_{1-y}Al_yCl_6$(x=0.05,y=0.2).

Table S1. Lifetime constants of $Cs_2Na_{1-x}Ag_xBi_{1-y}Al_yCl_6$(x=0.05)

| y | $\tau_1$/μs($A_1$) | $\tau_2$/μs($A_2$) | $\tau_{avr}$/μs |
|---|---|---|---|
| 0.05 | 2.16(0.35) | 5.77(0.65) | 5.16 |
| 0.1 | 2.63(0.6) | 7.23(0.4) | 5.69 |
| 0.2 | 2.91(0.57) | 7.73(0.43) | 6.11 |
| 0.3 | 2.97(0.66) | 8.54(0.34) | 6.30 |

Table S2 Comparison of performance of different NIR light emitters.

| composition | PL(nm) | PLQY(%) | FWHM(nm) | I(%)@Temp. | Refs |
|---|---|---|---|---|---|
| $Cs_2Na_{1-x}Ag_xBi1_{-y}Al_yCl_6$ | 715 | 49 | 259 | 51@340K | This work |
| $Na_3Al_2Li_3F1_2$: $Cr^{3+}$ | 750 | 78 | 110 | 99@423K | 60 |
| $NaInGe_2O_6$: $Cr^{3+}$ | 900 | 34 | 175 | 53@380K | 61 |
| $CaSc_{0.85}Al_{1.15}$ $SiO_6$: $Cr^{3+}$ | 950 | 33 | 205 | 77@380K | 62 |
| $NaScSi_2O_6$:$Cr^{3+}$ | 840 | — | | 81@423K | 63 |
| $CuInSe_2$@ZnS:Mn | 1071 | 31 | — | — | 64 |
| $CuInSe_2$@ZnS | 1224 | 22 | — | — | 65 |
| $LiScGe_2O_6$: $Cr^{3+}$ | 886 | 73 | 160 | 42@350k | 66 |
| $CaMgSi_2O_6$: $Cr^{3+}$ | 882 | 47 | 197 | 85@373K | 67 |
| $LiInO_2$ :$Cr^{3+}$ | 900 | 36 | 150 | — | 68 |


[1] Perdew, J. P.; Levy, M. Physical Content of the Exact Kohn-Sham Orbital Energies: Band Gaps and Derivative Discontinuities. *Phys. Rev. Lett.* **1983**, 51, 1884−1887

[2] G Kresse, J Furthmüller. Efficient iterative schemes for ab initio total-energy calculations using a plane-wave basis set. *Phys. Rev. B*. **1996**, *54* (16), 11169-11186.

[3] J P Perdew, K Burke, M Ernzerhof. Generalized gradient approximation made simple. *Phys. Rev. Lett*. **1996**, *77* (18), 3865-3868.

[4] P E Blöchl. Projector augmented-wave method. *Phys. Rev. B*. **1994**, *50* (24), 17953-17979